Antitumor Potential of new organo-metalic Compounds For Breast Cancer MCF-7 Cell Lines

Shaimaa M.Faheem[a], Abdou S. El-Tabl[b], Moshira M. Abd-El Wahed[c], Mohammed H. H. Abu-Setta[*d], Yousra H.El-Meligy[e] and Sara M. Younes[f]

[a] Higher Technological Institute of Applied Health Sciences, Badr Academy, Badr City,Cairo,Egypt.

[b,d,f] Department of Chemistry, Faculty of Science, El-Menoufia University, Shebin El Kom, Egypt.

[c] Department of Pathology, Faculty of Medicine, El-Menoufia University, Shebin El-Kom, Egypt.

[f] Chemical Engineering Department, Borg El Arab Higher Institute Engineering and Technology, Alexandria, Egypt.

* Corresponding author: E-mail address: dr.mohammedhosnyabusetta@gmail.com

ABSTRACT

New organometallic compounds of Mn(II), Fe(III), Ni(II), Cu(II), and Zn(II) (1Z,2Z)-N1,N'1,N2,N'2-tetrakis(2-hydroxyphenyl) oxalimidamide ligand have been prepared and characterised using elemental and spectral analyses, magnetic moments, conductance, and thermal analysis (DTA and TGA). The complexes were non-electrolytes based on molar conductance in DMF solutions (11.2 - 14.5 ohm^{-1} cm2 mol^{-1}). The ESR spectra of solid Cu(II) complexes (2), (3), and (4) revealed an axial type symmetry, indicating a b&a $d(x^2-y^2)$ ground state with a substantial covalent bond character, whereas Mn(II) complex(5) revealed an isotropic type.Furthermore, the spectra corroborated the octahedral structure of the metal ions. The complexes were tested for cytotoxicity as antitumor agents against breast cancer using the MCF-7 cell line. Cu(II) complex (2) outperformed Cu(II) complex (1) in terms of cytotoxicity against breast malignant cells. Cu(II) complex (2) had a stronger cytotoxic effect on breast malignant cells, with an IC50 of 7.5 ug.IC50 for a reference medicine (cisplatin) was 5.71 ug, Cu(II) complex (2)>Pb(II) complex (10)>Zn(II) complex (9), Cu(II) complex (4)>Cu(II) complex (3), Zn(II) complex (8)>Fe(III) complex (6)>Ni(II) complex (7) with IC50 within range (21-7.5 ug). Complexes outperformed the parent ligand and the standard medication (cisplatin) in terms of activity. These investigated complexes are potential anticancer drugs for the MCF-7 breast cancer cell line.

Keywords: Amide ligand , complexes, analysis ,spectra , magnetism , ESR, cytotoxicity, breast cancer.

Introduction

Metal complexes are tiny compounds that have been widely used as therapeutic agents, acting as biological agents with outstanding chemotherapeutic capabilities [1] . Cisplatin and its analogues were among the first clinically established and successful anticancer medications, and they efficiently attach to DNA, causing cell death [2] . Nonetheless, these drugs have negative side effects such as nausea, neurotoxicity, and nephrotoxicity [3]. Furthermore, overuse of these medications resulted in acquired or innate resistance to some cancer types. Because of the aforementioned factors, the scientific community has devoted significant time and effort to the design and development of novel chemotherapeutic agents that can disrupt or halt cancerous cellular mechanisms, with nucleic acids being targeted as the precursors aiding the process of cell replication. Nucleic acids are essential macromolecules that influence many biological activities[3,4]. According to the Watson and Crick model, DNA is a double helix structure wrapped in a right-handed way[5]. DNA is composed of a sugar-phosphate backbone and the nucleotide bases adenine (A), guanine (G), thymine (T), and cytosine (C), where these bases are joined by hydrogen bonding. [5-6] Minor and major grooves are seen in the DNA's double-helical structure. When the two strands are near together, minor grooves form, and when they are separated, major grooves form. These two DNA strands are made up of nucleotide bases. The complementary DNA strands run antiparallel to each other. The initial strand is made up of 5' OH groups. Small compounds or metal complexes bond to these nucleic acids, causing structural changes and the desired function, which can be utilised to detect and treat a variety of disorders.Cancer targeting techniques based on biomolecule-conjugated metal complexes have demonstrated enormous benefits in cancer therapy. where these bases are linked by hydrogen bonding [5-6] . In the double-helical structure of DNA, minor and major grooves may be detected. Minor grooves form when the two strands are close together, while major grooves emerge when they are separated. The nucleotide bases that make up these two DNA strands. The complementary DNA strands are orthogonal to one another. The first strand consists of 5' OH groups. Small chemicals or metal complexes link to these nucleic acids, creating structural changes and the desired activity, which can be used to detect and cure a wide range of diseases. Cisplatin's clinical use has been limited due to the occurrence of dangerous side effects such as nephrotoxicity, nevrotoxicity, and

2027

Eur. Chem. Bull. 2023,12(12), 2026-2058

cytotoxicity. The disadvantages of cancer therapy are primarily the lack of therapeutic specificity and the development of drug resistance. As a result, second-generation anticancer medications, such as metal-based complexes with a customised drug delivery mechanism, are being researched as prospective alternatives. Metal complexes for anti-breast cancer treatment, such as gold(III) complexes, platinum(II) complexes, ruthenium complexes, and cisplatin. Transition metal-based compounds are advantageous binding agents that demonstrate particular binding interactions with nucleic acids and a variety of other proteins, making them valuable in the field of chemotherapeutics [7] .Cancer targeting approaches based on biomolecule-conjugated metal complexes have shown tremendous promise in cancer treatment. Furthermore, the spectroscopic properties of transition metal-based probe molecules allow them to be used in numerous biophysical research relevant to the development of various anticancer medicines. The variable coordination numbers, redox potentials, and geometry that typical organic compounds cannot realise make these molecules unique among all anticancer medicines produced to date [8]. The ability of these probes (metal complexes) to read the information in the DNA duplex results in the efficient binding of these probes to DNA. Following binding, the probes are anchored into the DNA duplex by a variety of interactions including as stacking, hydrogen bonding, van der Waals forces, and so on. New organometallic compounds of (1Z,2Z)-N1,N'1,N2,N'2-tetrakis(2-hydroxyphenyl)oxalimidamide were synthesised and characterised as effective anticancer drugs.

Experiment

Materials and Instrumentation

All of the chemicals utilised to prepare the ligand and its complexes were synthetic grade and used without further purification. TLC was employed to establish the purity of the compounds[11]. The C, H, N, and Cl studies were performed at Cairo University's Analytical Unit in Egypt. Metal ions were identified using standard gravimetric techniques [10-12]. All metal complexes were vacuum-dried over P_4O_{10}. The IR spectra of KBr pellets were obtained using a PerkinElmer 683 spectrophotometer (4000-400 cm-1). A PerkinElmer 550 spectrophotometer was used to record qualitative electronic spectra. The conductance (10-3M) of the complexes in DMF were measured at 25C° using a Bibby conduct metre type MCl. The 1H-NMR spectra of the ligand and its Zn (II) complex were acquired using a PerkinElmer R32-90-MHz spectrophotometer with

2028

Eur. Chem. Bull. 2023,12(12), 2026-2058

TMS as an internal standard. The mass spectra were recorded using a JEULJMS-AX-500 mass spectrometer that included with the data system. Thermal studies (DTA and TGA) were performed in air on a Shimadzu DT-30 thermal analyzer from 27 to 800°C at a heating rate of 10C° per minute. Magnetic susceptibilities were measured using the Gouy method at 25C° with mercuric tetrathiocyanatocobalt(II) as the magnetic susceptibility standard. Pascal's constant[13] was used to calculate magnetic adjustments. The magnetic moments were estimated using the equation: eff = 2.828 (n T)1/2. The ESR spectra of solid complexes at room temperature were acquired using a Varian E-109 spectrophotometer with DPPH as a reference material.
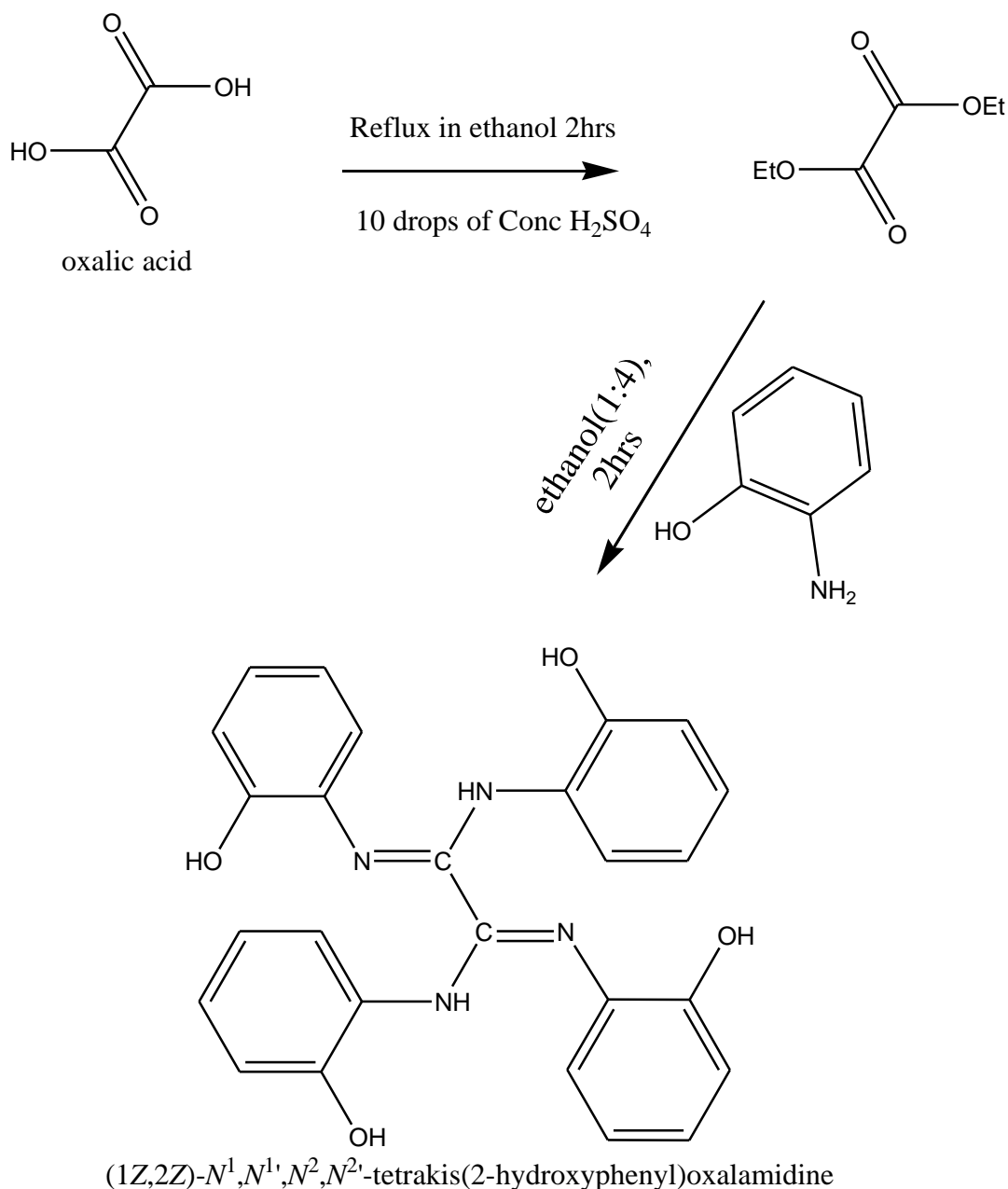
Prepration of ligand (1):

Prepration of diethyle oxalate:

Diethyle oxalate (scheme 1) was created by adding an equimolar quantity of oxalic acid (20g,1.0mole) to 200 cm^3 of absolute ethanol, followed by 10 drops of pure sulforic acid. The mixture was refluxed over a water bath for 2 hours and then allowed to cool at room temperature to yield diethyle oxalate.

Prepration of amide ligand ((1Z,2Z)-N1,N'1,N2,N'2-tetrakis(2-hydroxyphenyl)oxalimidamide:

The ligand (H4L) (1Z,2Z)-N1,N'1,N2,N'2-tetrakis(2-hydroxyphenyl) oxalimidamide (scheme 1) was synthesised by combining diethyl oxalate (5.0 g, 0.034 mole) with ortho hydroxyl aniline (14.93 g, 0.136 mole) in 70 cm^3 of pure ethanol (1:4). For two hours, the mixture was refluxed while stirring. After cooling to ambient temperature, the solvent was extracted under decreased pressure, yielding crude product, which was crystallised in ethanol to yield pure ligand (1): yield 75%, m.p.224 c, lustrous brown colour.

2029

Eur. Chem. Bull. 2023,12(12), 2026-2058

$(1Z,2Z)$-N^1,$N^{1'}$,N^2,$N^{2'}$-tetrakis(2-hydroxyphenyl)oxalamidine

Schem 1. Prepration of amide ligand ((1Z,2Z)-N1,N'1,N2,N'2-tetrakis(2-hydroxyphenyl)oxalimidamide

Preparation of metal complexes (2)-(12)

The metal complexes were made in a (1L:2M) molar ratio by continuously swirling an appropriate amount (2.0 mol) of a heated ethanolic solution of the metal salts: $Cu(CH_3COO)$ (2), $CuSO_4.5H_2O$ complex (3), $CuCl_22H_2O$ complex (4), and $Mn(CH_3COO).FeSO_47H_2O$ compound (6), $Ni(CH_3COO)$ complex (5)$Zn(CH_3COO)$ complex (7), $24H_2O$ complex (7)$2H_2O$ complex (8), $ZnSO_4.7H_2O$ complex (9), $Pb(SO4)_2$ complex (10), $MnCO_3$ complex (11) and $MnSO_4$ complex (12) in a hot ethanolic solution of the ligand (1 mol, 30 mL ethanol). Depending on the type of the

2030

metal ion, the refluxing times ranged from 2 to 4 hours. The produced precipitates were filtered out, washed with ethanol, then with diethyl ether, and dried in vacuum desiccators over P_4O_{10}.

Results and discussion

All of the metal complexes are stable at room temperature, insoluble in water, non-hydroscopic, moderately soluble in MeOH, EtOH, $CHCl_3$ and $(CH_3)_2CO$, and completely soluble in DMF and DMSO [14]. The analytical and physical data, as well as the spectrum data (experimental component, Tables 1 and 2), are consistent with the proposed structures (Figures 1-4). The complexes' molar conductance in 10^{-3} M DMF at 25 C° was in the 11.2-14.5 ohm-1cm^{2}mol^{-1} range, indicating a non-electrolytic nature. These low values reflect the absence of counter ions in their structure [15]. Many attempts have been made to grow a single crystal up to this point, but all have failed. Complexes (2-12) were produced by reacting the ligand (1) with metal salts in ethanol at room temperature.

Table 1 :- Analytical and physical data of ligand **(1)** and its metal complexes **(2-12).**

No.	Ligand/Complexes	Color	FW	M.P (^{O}C)	Yield (%)	Anal. /Found (Calc.) (%)				Conductivity Λ
						C	H	N	M	
(1)	**$C_{26}H_{22}O_4N_4 . H_2O$** [H$_4$L]H$_2$O	Shiny brown	472	141	97	67.20 (67.4)	4.26 (4.97)	12.97 (12.1)	-	-
(2)	**$C_{34}H_{40}O_{15}N_4CU_2$** [(H$_4$L)(cu$_2(OAC)_4$)].3H$_2$O	**Shiny black**	871	**333**	95	46..93 (**46.84**)	4.77 (4.59)	6.59 (**6.42**)	14.66 (**14.58**)	13.50
(3)	**$C_{26}H_{26}O_{14}N_4CU_2S_2$** [H$_4$L .cu$_2$(SO$_4$)$_2$]. 2H$_2$O	black	809	**301**	90	38.67 (38.56)	3.05 (3.2)	7.56 (6.9)	15.8 (15.69)	13.7
(4)	**$C_{26}H_{28}O_6N_4CU_2CL_4$** [(H4L)(cu$_2CL_4$)].2H$_2$O	black	761	**325**	**96**	40.88 (40.99)	3.62 (3.67)	7.33 (7.35)	16.67 (16.68)	13.2
(5)	**$C_{34}H_{38}O_{14}N_4Mn_2$** [H$_4$L.(Mn$_2(OAc)_4$)].2H$_2$O	Light Coffe brown	836	**302**	93	48**1.** (48.8)	4.5 (4.54)	6.61 (6.69)	13.20 (13**.**16)	1450.
(6)	**$C_{26}H_{26}O_{14}N_4Fe_2S_2$** [H$_4$L.(Fe $_2$(so$_4$)$_2$(H$_2$o)$_2$].2H$_2$O	black	832	**309**	**90**	39.38 (39.2)	3.83 (3.3)	7.14 (7.03)	14.5 (14.3)	12.8
(7)	**$C_{34}H_{38}O_{14}N_4Ni_2$** [H$_4$L.(Ni $_2$(OAc)$_4$)].2H$_2$O	**Shiny black**	843	**317**	84	48.43 (48.38)	4.23 (4.5)	6.71 (6.64)	13.91 (13.92)	12.9
(8)	**$C_{34}H_{38}O_{14}N_4Zn_2$** [(H$_4$L).Zn$_2(OAc)_4$)] .2H$_2$O	Light green	856	**310**	**97**	47.02 (47.6)	4.55 (4.44)	6.69 (6.54)	15.10 (15.26)	11.20
(9)	**$C_{26}H_{26}O_{14}N_4Zn_2S_2$** [(H$_4$L).Zn$_2$ (SO$_4$)$_2$].2H$_2$O	grey	812	**305**	**85**	38.60 (38.1)	3.65 (3.2)	6.9 (6.89)	16.4 (16.1)	**12.50**

2031

Eur. Chem. Bull. 2023,12(12), 2026-2058

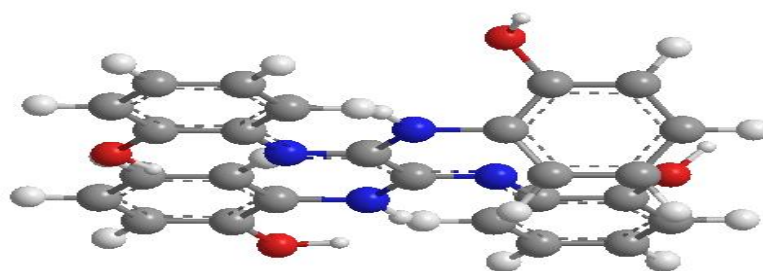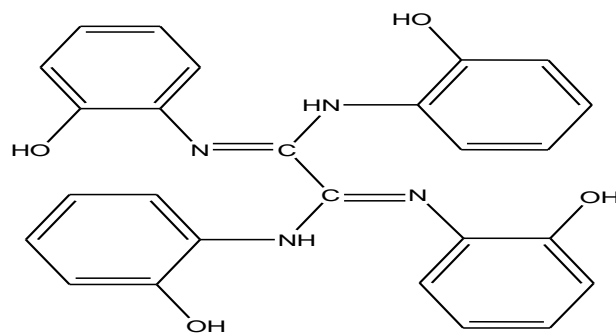|									
(10)	$C_{26}H_{26}O_{14}N_4Pb_2S_2$ [$(H_4L).(Pb_2(SO_4)_2(H_2o)_2$].2H_2O	Light brown	1132.4	**340**	86	27.5 (27.46)	2.65 (2.37)	4.95 (5.11)	37.25 (37.79)	12.60
(11)	$C_{28}H_{26}O_{12}N_4Mn_2$ [$(H_4L).Mn_2(CO_3)_2(H_2o)_2$].2H_2O	Shiny brown	756	**315**	90	44.4 (44.6)	3.96 (3.60)	7.41 (7.70)	15.41 (15.27)	12..1
(12)	$C_{26}H_{26}O_{14}N_4Mn_2S_2$ [$(H_4L).Mn_2(SO_4)_2(H_2o)_2$].2H_2O	Off white	828	**312**	92	37.68 (37.4)	3.62 (3.28)	6.76 (7.07)	8.75 (**80**.8)	12.40

$Ohm^{-1} cm^2 mol^{-1}$

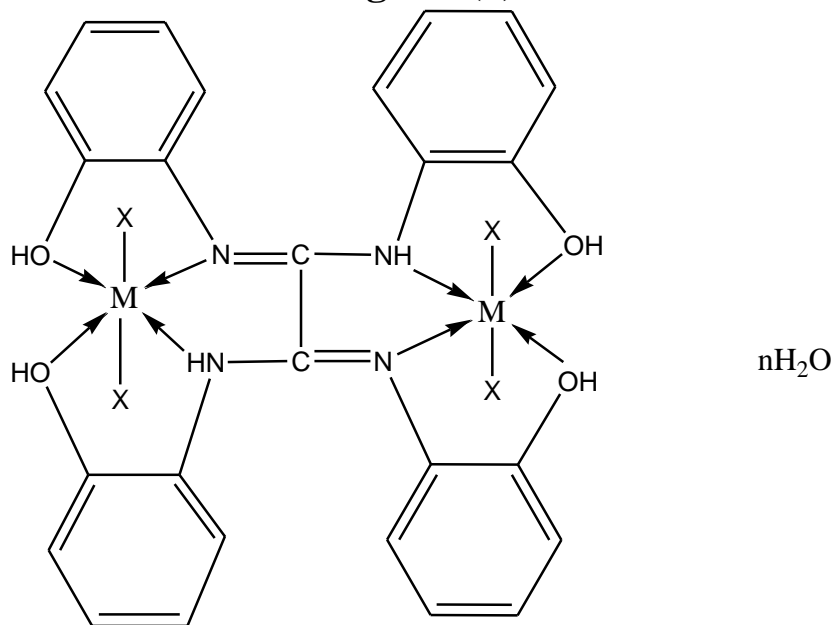## ^{1}H-NMR spectra of the ligand (1) and complexes (8-10)

The ^{1}H-NMR spectra of the ligand and its complexes (8-10) in deuterated DMSO revealed peaks compatible with the hypothesised structure[16].The ligand's ^{1}H-NMR spectra revealed a chemical shift detected as a singlet at 9.7 ppm, which was assigned to a proton of aromatic hydroxyl groups. The chemical shift at 3.17 ppm was attributed to the proton of NH linked to (CH- of aromatic ring); (C=N-Ar-). However, a group of signals showed as multiples in the 6.4-6.6 ppm range, matching to aromatic ring protons.By comparing the ^{1}HNMR spectra of the ligand and the complexes (8-10); signal was discovered as a singlet at 10.0 ppm distinctive to the OH group indicating that the ligand was identified in the protonated state. Furthermore, a considerable downfield shift of the NH linked to (CH- of aromatic ring); (C=N-Ar-) proton signal relative to the free ligand revealed that metal ions are coordinated to the amide nitrogen atom. This change could be the result of the development of a coordination bond (N-M) [16,17] **(Scheme 1& Figure 2).**

The structures of the metal complexes

From all previous analyses and tests on the metal complexes, it was found that, their chemical structures were as follows
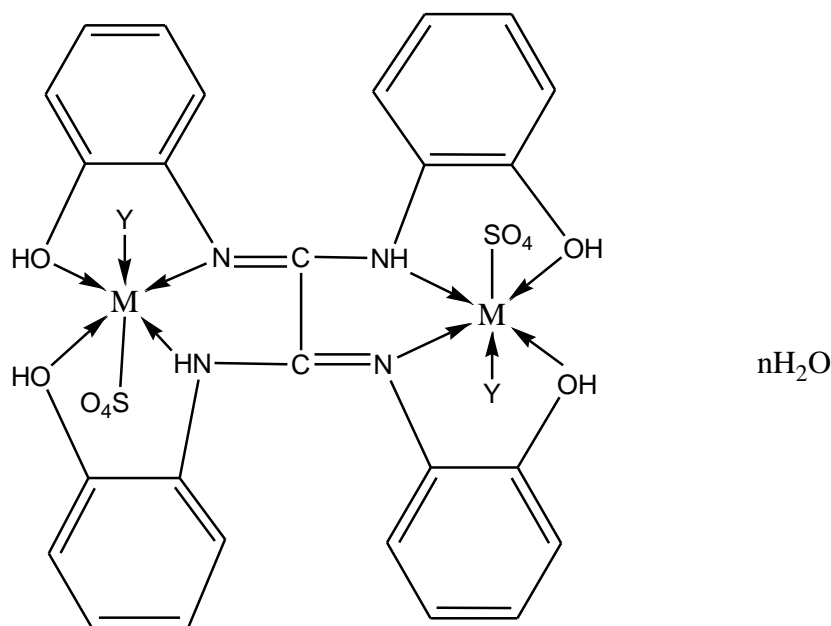
2032

Eur. Chem. Bull. 2023,12(12), 2026-2058

(1Z,2Z)-N^1,$N^{1'}$,N^2,$N^{2'}$-tetrakis(2-hydroxyphenyl)oxalamidine

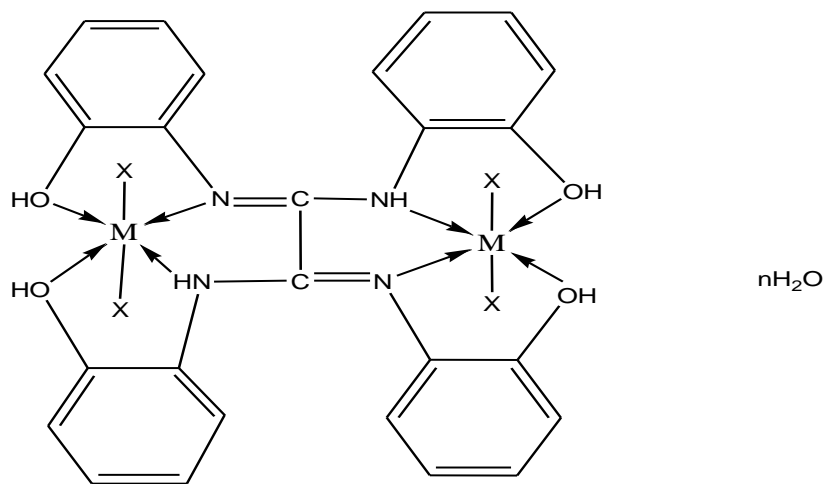**Ligand (1)**

nH$_2$O

M=Cu(II), X= OAc, n=3, Complex (2)
M=Mn(II) , X= OAc , n=2, Complex (5)
M=Ni(II) ,   X= OAc , n=2, Complex (7)
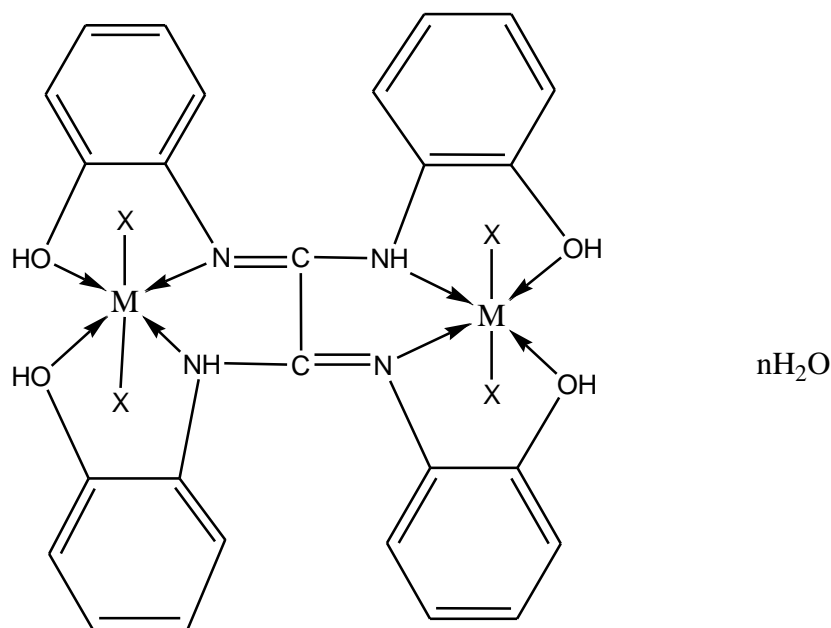**M=Zn(II) , X= OAc , n=2, Complex (8)**

2033

Eur. Chem. Bull. 2023,12(12), 2026-2058

M=Cu(II), X= SO$_4$, Y= H$_2$O , n=2, Complex (3)
M=Fe(II) , X= SO$_4$, Y= H$_2$O , n=2 , Complex (6)
M=Zn(II) , X= SO$_4$,Y= H$_2$O , n=2,   Complex (9)
M=Pb(II) , X= SO$_4$, Y= H$_2$O , n=2 , Complex (10)
M=Mn(II), X= SO$_4$,Y= H$_2$O , n=2 , Complex (12)

M=Cu(II), X= Cl, n=2 , Complex (4)

2034

Eur. Chem. Bull. 2023,12(12), 2026-2058

M=Mn(II), X= CO$_3$, n=2 , Complex **(11)**

Fig. 1: Structure representation of metal complexes **(2-12)**

IR spectra

The method of bonding between the ligand and the metal ion is revealed by comparing the IR spectra of the ligand (1) and its metal complexes (2-12). The ligand exhibited bands in the 3660-3190 and 3160-2500 cm^{-1} ranges, indicating the presence of two types of intra- and intermolecular hydrogen bonding of OH and NH groups with imine groups [15-17]. As a result, the higher frequency range was associated with a weaker hydrogen bond. The medium band at 3200 cm^{-1} was assigned to the v(NH) group [18-19]. The υ (NH) group emerged at distinct regions of the free ligand in the complexes, indicating that the NH group is involved in metal ion coordination [20]. The υ (CN) vibration was responsible for the appearance of strong bands at 1632 and 1625 cm^{-1}. The bands seen at 1578,780, 1550, and 750 cm^{-1} were ascribed to υ (Ar) vibration [20,21]. By comparing the IR spectra of the complexes (2-12) with that of the free ligand. It was discovered that the position of the υ (NH) bands in complexes was changed by 3159-3190 cm^{-1} range towards lower wave number, indicating coordination through nitrogen of NH group [20,21]. The υ (CN) groups emerged in the 1602-1625 cm^{-1} range, indicating that the υ (CN) group was engaged in the coordination to the metal ion [20]. This is further supported by the presence of additional bands in the 520-580 cm^{-1} range, which have been attributed to the υ (M-N)

2035

Eur. Chem. Bull. 2023,12(12), 2026-2058

[21]. In acetate complexes (2), (5), (7), and (8), bands were detected in the (1450,1435 cm^{-1}),(1438,1330 cm^{-1}),(1450,1342cm^{-1}) and(1450,1320 cm^{-1}) respectively, indicating monodentate coordination of the acetate group in these complexes [18,22].Sulphato complexes (3),(6),(9),(10), and (12) displayed bands at (1175,1125,1015,680 cm^{-1}), (1170,1130,1025,675 cm^{-1}), (1180,1145,1030,680 cm^{-1}), (1170,1138,1019,675 cm^{-1}) and (1020,1168,1132,681 cm^{-1}) attributed to the monodentate sulphate group [23]. Complexe (11), which has bands 1670, 1645, and 1242 cm^{-1}, has been classified to the CO_3 group. Complexes (2)-(11) exhibit bands in the 520-580 cm^{-1} range, which was attributed to υ (M-N) [22]. Complexes (2-11) displayed bands in the 604-633 range.

2036

Eur. Chem. Bull. 2023,12(12), 2026-2058

Table 2:- IR Frequencies of the bands (cm^{-1}) of the ligand **[H₄L] (1)** and its metal complexes

No.	ν(H$_2$O)	ν(OH)	υ(H-bonding)	ν(NH)	ν(C=N)	ν(Ar)	ν(OAc)/SO$_4$/CO$_3$	υ(M-O)	ν(M-N)	υ(M-Cl)
Ligand (1)	3360-3190	3500, 3425, 1320	3660-3170 , 3160-2500	3200	1632, 1625	(1578,780) , (1550,750)	-	-	-	-
Complex (2)	3370-3260 1300-1180	3432 , , 1290	(3610-3220) , (3210-2790)	3159	1625	(1549-1555) , (780-790)	1450,1435	610	535	-
Complex (3)	3360-3250 3240-3120	3420, 3385, 1285	(3650-3190) , (3180-2650)	3180, 3162	1620, 1612	(1575,780 ,1555,735)	1175,1125,1015,680	620	580	-
Complex (4)	3305-3170	3395, 1270	(3580-3210) , (3210-2650)	3177	1617, 1605	(1500,1482 ,780, 751)	-	633	580	448
Complex (5)	3350-3210,	3408-1242	3590-2220 3210-2775	3180	1617, 1609	1520,1500 735,765	1438,1330	615	560	-
complex (6)	3400-3600 , 3300-3190	3420 , 1239	(3660-3320) , (3210-2820)	3190	1610 ,1602	(1490,1460) , (750,742)	1170,1130, 1025,675	630	570	-
complex (7)	(3380-3200) ,	3370, 3350, 1741	(3610-3250) , (3240-2900)	3170	1615 ,1603	(1400,1450) , (730,743)	1450,1342	610	560	-
Complex (8)	(3380-3320)	3379, 1254,	(3600-3200), (1320-1050)	3175	1617, 1608	(1557,1490 ,874, 725)	1450,1320	630	520	-
complex (9)	(3350-3190) ,(3180-3090)	3356, 1290,	(3650-3310) , (3300-2820)	3175	1617, 1600	1500,1462 ,720,742	**1180,1145,1030,680**	610	560	-
complex (10)	(3390-3210) ,(3200-3130)	3400 ,3355,1270,	(3600-3320), (3110-2700)	3162	1615 ,1603	1510 ,770	**1170,1138,1019,675**	605	580	-
Complex (11)	3410-3250 3280-3070	3400-1275	3570-3310 3300-2700	3190	1616, 1605	1549,1500, 780,760	**1670,1645,1242**	615	580	-
complex (12)	(3390-3230) , (3270-3120)	3373, 1280	(3610-3280) , (3250-2800)	3162	1618, 1602	(1510,1493) , (790,747)	**1168,1132,1020,681**	604	552	-

2037

Eur. Chem. Bull. 2023,12(12), 2026-2058

Magnetic moments

(Table3) shows the magnetic moments of the metal complexes (2)-(12) at room temperature. Cu(II) complexes (2-4) had values in the 1.69-1.71 B.M. range, which corresponded to one unpaired electron in an octahedral structure [25,26]. Manganese(II) complexes (5) and (12) have B.M values of 5.93 and 6.3, respectively, indicating high spin octahedral geometry around the Mn(II) ion [18,26]. The value of Ni(II) complex (7) was 3.26 B.M, indicating an octahedral Ni(II) complex [27]. Complexes of Zn(II) (8),(9). Pb(II) complexes (10) exhibited diamagnetic behaviour [26,27]. The Fe(III) complex (6) had a B.M of 6.37, indicating a high spin octahedral structure.

Mass spectra

Ligand (1) [H4L] and its its metals, Cu(II) complex (2) ,Mn(II) complex (5), Fe(III) complex (6), Zn(II) complex (8), Zn(II) complex (9), Mn(II) complex (11) and Mn(II) complex (12) mass spectra confirmed their predicted formulation[28]. The spectra of Ligand (1) revealed a molecular ion peak (m z) at 472 amu, which was consistent with the ligand's molecular weight, confirming its formula weight (F.W. 472). Furthermore, the pieces detected at (m z) = 92, 118, 122, 134, 278, 391, 413, 455, and 473 amu correspond to the moieties C_6H_4O, C_7H_4ON, $C_7H_8 ON$, C_8H_8ON, $C_{15}H_8O_3N_3$, $C_{23}H_{11}O_3N_4$, $C_{24}H_{21}O_3N_4$, $C_{26}H_{23}O_4N_4$, and $C_{26}H_{25}O_5N_4$. Complex (2)'s mass spectrum revealed a molecular ion peak at m/z 871 amu, validating its formula weight (F.W. 871). The measured mass fragmentation patterns at m/z = 91,301,414,507,639,683and870 amu correspondtoC_7H_7,,$C_{16}H_{15}O_5N$,$C_{20}H_{15}O_9N_3$,$C_{30}H_{31}O_{12}N_4$,$C_{31}H_{31}O_{14}N_4$ and $C_{34}H_{40}O_{15}N_4Cu_2$ moieties, respectively, and validated the complex's proposed structure.Complex (5)'s mass spectrum revealed a molecular ion peak at m/z 836 amu, validating its formula weight (F.W. 836).The mass fragmentation patterns obtained at m/z=71,205,301,413,460,590,639,742,and834amucorrespondtoC_5H_{11},$C_{12}H_{13}O_3$,$C_{15}H_{27}O_5N$,$C_{19}H_{29}O_8N_2$,$C_{19}H_{30}O_{10}N_3$,$C_{26}H_{30}O_{12}N_4$,$C_{30}H_{31}O_{12}N_4$,$C_{34}H_{32}O_{12}N_4Mn$ and$C_{34}H_{38}O_{14}N_4Mn_2$ moieties, respectively, corroborated the hypothesised structure of the complex. Complex (6)'s mass spectrum revealed a molecular ion peak at m/z 796amu, validating its formula weight (F.W.796).The measured mass fragmentation patterns at m/z =71,122,205,301,413,507,638, and768 amu correspond to C_5H_{11},

$C_8H_{10}O$, $C_{12}H_{13}O_3$, $C_{16}H_{15}O_5N$, $C_{20}H_{15}O_9N$, $C_{20}H_{15}O_{12}N_2S$, $C_{22}H_{23}O_{13}N_4SFe$, and $C_{24}H_{26}O_{14}N_4S_2Fe_2$ moieties, respectively.Complex (8)'s mass spectrum revealed a molecular ion peak at m/z856 amu, validating its formula weight (F.W. 856).The mass fragmentation patterns observed at m/z = 71,149,267,301,413,507,590,678, 743, and 856 amu correspond to C_5H_{11}, $C_{10}H_{13}O$, $C_{14}H_{19}O_5$, $C_{15}H_{27}O_5N$, $C_{19}H_{29}O_8N_2$, $C_{23}H_{29}O_{10}N_3$, $C_{26}H_{30}O_{12}N_4$, $C_{33}H_{34}O_{12}N_4$, $C_{33}H_{34}O_{12}N_4Zn$ and $C_{34}H$.

The complex (9) mass spectrum revealed a molecular ion peak at m/z 812 amu, validating its formula weight (F.W. 812).The mass fragmentation patterns observed at m/z =90, 122, 134, 198,301,413,463, 507,551, 683 and 808 amu correspond to C_7H_6,$C_7H_6O_2$, $C_8H_6O_2$, $C_{12}H_8O_2N$, $C_{16}H_{15}O_5N$, $C_{20}H_{15}O_9N$, $C_{20}H_{19}O_9N_2S$,$C_{21}H_{19}O_{11}N_2S$, $C_{22}H_{21}O_{12}N_3S$,$C_{22}H_{21}O_{12}N_3S$,$C_{25}H_{22}O_{13}N_4SZn$ and$C_{26}H_{22}O_{14}N_4S_2Zn_2$ moieties, respectively, supported the suggested structure of the complex. However, the complex (11) mass spectrum revealed a molecular ion peak at m/z 720 amu, validating its formula weight (F.W. 720).The mass fragmentation patterns reported at m/z = 91,110,149,213,301,391,479,551 , 683 and718 amu correspond to C_7H_7, $C_7H_{10}O$, $C_9H_{11}ON$, $C_9H_{11}O_5N$, $C_{15}H_{11}O_6N$, $C_{17}H_{15}O_9N_2$, $C_{23}H_{15}O_{10}N_2$, $C_{26}H_{23}O_{10}N_4$, $C_{28}H_{23}O_{10}N_4Mn_2$ and$C_{28}H_{26}O_{12}N_4Mn_2$ moieties, respectively, corroborated the hypothesised structure of the complex. The mass spectrum of complex (12) revealed the molecular ion peak at m/z 792amu, validating its formula weight (F.W. 792).The mass fragmentation patterns observed at m/z = 71,149,301,413,507,546,590,634,678 ,733and 792 amu correspond to C_5H_{11}, $C_9H_{11}ON$, $C_{15}H_{11}O_6N$, $C_{19}H_{13}O_9N_2$, $C_{23}H_{13}O_{11}N_3$, $C_{23}H_{20}O_{13}N_3$, $C_{24}H_{20}O_{13}N_3S$, $C_{25}H_{20}O_{13}N_3S_2$, $C_{26}H_{22}O_{14}N_4S_2$,$C_{26}H_{22}O_{14}N_4S_2Mn$ and $C_{26}H_{26}O_{14}N_4S_2Mn_2$ moieties, respectively, supported the suggested structure of the complex.respectively, backed up the complex's proposed structure.

Electronic spectra

Table 3 summarises the electronic spectrum data for the ligand (1) and its metal complexes in DMF solution. Ligand (1) in DMF solution exhibited four bands at 400 nm (=9.65 x 10^{-3} mol^{-1} cm^{-1}), 320 nm (=7.72 x 10-3 mol-1 cm^{-1}), 302 nm (=7.28 x 10^{-3} mol^{-1} cm^{-1}) and 292 nm (= 7.04 x 10^{-3} mol^{-1} cm^{-1}) that may be assigned to n→π* , π→π* transitions of the immine and aromatic ring [29]. Cu(II) complexes (2-4) showed bands at 283 and 302-305 nm, which were due to intra-ligand transitions; however, bands at 475-425, 570-560, and 625-605 nm were assigned of O to Cu,

2039

Eur. Chem. Bull. 2023,12(12), 2026-2058

charge transfer, $^2B^1$ to ^2E, and $^2B^1$ to $^2B^2$ transitions, indicating a tetragonal octahedral structure [30,31]. However, Mn(II) complexes (5),(11) and(12) showed bands in the 285-205, 300-300, 465-485, 585-570 ranges and 640-612 nm, the first bands were within the ligand and the other bands are assigned $^6A_1g{\rightarrow}^4Eg$, $^6A_1g{\rightarrow}^4T_2g$ and $^6A_1g{\rightarrow}^4T_1g$ transitions which were compatible to an octahedral geometry around the Mn(II) ion [26,30]. Pb(II) complexes (10) and Zn(II) complexes (8) and (9) revealed intra-ligand transition bands. However, Ni(II) complex (7) showed bands in the 290,300,340,370,480,530,640 nm ranges, the first three bands were within the ligand and the other bands are attributable to O→Ni charge transfer,$^3A_2g(F){\rightarrow}^3T_1g(P)$ (υ 3), $^3A_2g(F){\rightarrow}^3T_1g(F)$ (υ 2) and $^3A_2g(F){\rightarrow}^3T_2g(F)$ (υ 1) transitions respectively, indicating an octahedral Ni(II) geometry [30,32].

Table 3: Electronic spectra (nm) and magnetic moments (B.M) for the Ligand and Its complexes.

No.	Ligand/Complexes	λ_{max} (nm)	μ_{eff} (BM)
(1)	[H$_4$L]	290 nm (log ε =3.98),310 nm (log ε =4.25)	-
(2)	[(H$_4$L)Cu(H$_2$O)(OAc)$_2$].H$_2$O	283,305,475,568,610	1.70
(3)	[(H$_4$L)Cu(H$_2$O)(SO4$_2$].H$_2$O	285,305,425,472,560,605	1.69
(4)	[(H$_4$L) Cu (Cl)$_2$(H$_2$O)]. H$_2$O	260,300,435,575,610	1.71
(5)	[(H$_4$L) Mn(OAc)$_2$(H$_2$O)].2H$_2$O	285, 302, 485, 515, ,570, 625	5.93
(6)	[(H$_4$L)Fe(H$_2$O)(SO$_4$)$_2$].2H$_2$O	285,298,395,483,582,612	6.37`
(7)	[(H$_4$L) Ni (OAc)$_2$ (H$_2$O)]	290,300,340,370,480, 530, 640,740	3.26
(8)	[(H$_4$L) Zn (OAc)$_2$(H$_2$O)]. H$_2$O	265,288,308	Diamagnetic
(9)	[(H$_4$L) Zn(SO$_4$)$_2$(H$_2$O)] . 2H$_2$O	260,280,308	Diamagnetic
(10)	[(H$_4$L) Pb(SO$_4$)$_2$(H$_2$O)] . 2H$_2$O	265,286,306	Diamagnetic
(11)	[(H$_4$L) Mn(CO$_3$)$_2$(H$_2$O)] . H$_2$O	282,305, 435, 465,582, 612	1.69
(12)	[(H$_4$L)Mn (SO$_4$)$_2$(H$_2$O)].2H$_2$O	285,300,425,545,605	6.3

Electron spin resonance (ESR)

Table 3 shows the ESR spectrum data for complexes (2-4). Cu(II) complex spectra (3-5) were typical of the species d9 configuration with an axial type of a $d(x^2-y^2)$ ground state, which is the most frequent for copper(II) complexes [26,33]. The complexes exhibited $g_{\parallel}{>}g_{\perp}{>}2.0023$, indicating octahedral geometry surrounding the copper(II) ion [34,35].The expression $G = (g_{\parallel}-2)/ (g_{\perp} -2)$[33,34] connects the g-values,

2040

Eur. Chem. Bull. 2023,12(12), 2026-2058

where (G) exchanges the coupling interaction parameter (G). If G is less than 4.0, there is considerable exchange coupling, whereas if G is greater than 4.0, local tetragonal axes are parallel or just slightly misaligned. Complexes (2), (3), and (4) had values of 3.17, 3.6, and 3.28, respectively, confirming spin-exchange interactions amongst copper(II) ions.

The σ – parameter (α^2) was calculated from the following equations

α2= (g$_∥$ -2.0023)+3/7(g$_⊥$-2.0023)-(P)+0.04………………….………(1)

Where P is the free ion dipolar term which is equal 0.036, $A_∥$ is the parallel coupling constant expressed in cm^{-1}. The α^2 values of the copper complexes lie in 0.64 and 0.74 (Table 5], these values indicate to the presence of a significant degree in-plane σ covalence.

Where $k_∥$ and k are the parallel and perpendicular components of the orbital reduction factor (K), ° is the spin-orbit coupling constant for free copper, and Exy and Exz are the electron transition energies of $^2B^1 \rightarrow ^2B^2$ and $2B^1 \rightarrow ^2E$, respectively. The orbital reduction factors are derived from the above relationships.

($K_∥$, $K_⊥$, K), which are measure words for covalency [38], can be determined. In an ionic environment, K=1; in a covalent environment, K1. The higher the covalency, the lower the value of K.

K^2 = (g- 2.002) E$_{xz}$ /2°   **(2)**

$K_∥^2$ = (g$_∥$ - 2.002) E$_{xy}$ /8°   **(3)**

$K_⊥^2$ = ($K_∥^2$ +2K⊥^{2})/3   **(4)**

K values (Table 4) for copper(II) complexes (2), (3), and (4) indicate covalent bonding [26]. Kivelson and Neiman observed that g∥2.3 for an ionic environment and g∥2.3 for a covalent environment [35]. Smith's theoretical work appears to support this viewpoint. The g-values presented here (Table 4) demonstrated significant covalent bond nature [38]. In addition, the in-plane -covalency parameter, 2(Cu), was computed as 2 (Cu) = (A∥/0.036)+(g∥-2.002)+3/7(g -2.002)+0.04 (6).

Table 2 showed that the estimated values indicated covalent bonding [26]. In the following equations [30,36], the in-plane and out-of-plane -bonding coefficients 12 and 2 are dependent on the values of Exy and Exz.

$$\alpha^2\beta^2 = (g_⊥ - 2.002)\Delta E_{xy} / 2\lambda_o \text{ (5)}$$

$$\alpha^2\beta_1^2 = (g_{||} - 2.002)\Delta E_{xz} / 8\lambda_o \text{ (6)}$$

2041

Eur. Chem. Bull. 2023,12(12), 2026-2058

The complexes (2), (3), and (4) in this study had B212 values of 0.83, 1.05, and 1.17, indicating a considerable degree of covalency in the in-plane -bonding [38].The B2 values for complexes (2), (3), and (4) were 1.18,1.26, and 1.13, respectively, showing the ionic character of the out-of-plane, [17,39]. Approximate orbital populations for d orbitals [40] can be calculated using $A\| = A_{iso} - 2B[1 (7/4) g\|]$ $g= g- g_e$ (9),$d^2 =2B/ 2B°$ (10)

Where A° and 2B° are the predicted dipolar couplings for unit occupancy of the d orbital. The components of the Cu hyperfine coupling were evaluated with all sign combinations when the data was analyzed [40,41]. When A and A are both negative, the only physically significant outcomes are found. In this study, the complexes (2), (3), and (4) had B212 values of 0.83, 1.05, and 1.17, indicating a considerable degree of covalency in the in-plane -bonding [38].The B2 values for complexes (2), (3), and (4) were 1.18, 1.26, and 1.13, respectively, showing the ionic character of the out-of-plane, [17,39]. It is possible to derive estimated orbital populations for d orbitals [40] by **$A\| = A_{iso} - 2B[1 (7/4) g\|]$ $g= g- g_e$ (9),$d_2 =2B/ 2B°$ (7)**

Where A° and 2B° are the predicted dipolar couplings for unit occupancy of the d orbital, respectively. When analysing the data, the components of the Cu hyperfine coupling were considered in all sign combinations[41]. When A and A are both negative, the only physically significant results are obtained.

Table 4:-ESR data for some metal (II) complexes:-

No.	$g_\|$	$g_\perp$	g_{iso} [a]	$A_\|$ (G)	$A_\perp$ (G)	A_{iso} [b] (G)	G [c]	ΔE_{xy}	ΔE_{xz}	$K_\perp^2$	$K_\|^2$	K	K^2	$g_\|/A_\|$	α^2	β^2	β_1^2	2β	a_d^2 (%)
(2)	2.19	2.06	2.10	125	5	45	3.17	18018	20790	0.72	0.51	0.8	0.65	168.5	0.64	1.18	0.83	-209.8	89.27
(3)	2.22	2.06	2.11	100	10	40	3.6	18182	20833	0.72	0.6	0.80	0.64	222	0.57	1.26	1.05	-179.49	76.38
(4)	2.23	2.07	2.12	120	7.5	45	3.28	17483	21505	0.71	0.74	0.84	0.72	185.8	0.63	1.13	1.17	-211.5	90.0
(5)	-	-	2.03	-	-	-	-	-	-	-	-	-	-	-	-	-	--	-	-
(6)	-	-	2.01	-	-	-	-	-	-	-	-	-	-	-	-	-	-	-	-
(11)	-	-	2.05	-	-	-	-	-	-	-	-	-	-	-	-	-	-	-	-
(12)	-	-	2.01	-	-	-	-	-	-	-	--	-	-	-	-	-	-	-	-

a) $g_{iso} = (2g_\perp + g_\|)/3$, b) $A_{iso} = (2A_\perp + A_\|)/3$, c) $G= (g_\| - 2)/ (g_\perp - 2)$

2042

Eur. Chem. Bull. 2023,12(12), 2026-2058

Thermal analyses (DTA and TGA):

Thermo gravimetric curves of complexes (**2**),(**6**),(**8**),(**10**) **and**(**11**) were introduced as representative examples. Complex (**2**) **[H₄L (Cu) ₂(OAc)₄].3H₂O** exhibited multiple decomposition steps, the first step involving breaking of H-bonding accompanied with endothermic peak at 30°C. In the second step, three molecules of hydrated water molecules were lost endothermically with a peak at 65 C° accompanied by 5.9% (Calc 6.2%) . Weight loss. 28.7% (Calc 28.9%) weight loss accompanied by an endothermic peak at 285 C° was assigned to loss of four coordinated acetate groups (OAc). The endothermic peak observed at 310 °C refers to the melting point of the complex[42,43]. The final step observed as exothermic peaks at 425- 470 °C range with 27.12% weight loss (Calc 27.37%), refers to complete oxidative decomposition of the chelate which ended up with the formation of 2 (CuO69- . Complex (**6**) **[H₄L (Fe) ₂(SO₄)₂ (H₂O)₂].** **2H₂O** exhibited multiple decomposition steps, the first step involving breaking of H-bonding accompanied with endothermic peak at 35 C°. In the second step, two molecule of hydrated water were lost endothermically with a peak at 85 C° accompanied by 4.20% (Calc 4.35%) weight loss., then two molecule of coordinated water were lost endothermically with a peak at 135 C⁰ accompanied by 4.5% (Calc %4.55) weight loss. 25.43 (Calc 25.04%) weight loss accompanied by an endothermic peak observed at 331 C° was assigned to loss of two coordinated sulphate group (SO₄). The endothermic peak observed at 350°C refers to the melting point of the complex. The final step observed a exothermic peaks at 520-620 °C range with 25.2% weight loss (Calc 25.43%), refers to complete oxidative decomposition of the complex which ended up with the formation of 2(FeO)[44].

Complex (**8**) **[H₄L (Zn) ₂(OAc)₄].** **2H₂O** exhibited multiple decomposition steps, the first step involving breaking of H-bonding accompanied with endothermic peak at 42 C°. In the second step, two molecule of hydrated water were lost endothermically with a peak at 70 C° accompanied by 4.11% (Calc 4.13%) weight loss. 28.1 % (Calc 28.29%) weight loss accompanied by an endothermic peak observed at 235 C° was assigned to loss of four coordinated acetate groups (OAc). The endothermic peak observed at 350°C refers to the melting point of the complex. The final step observed a exothermic peaks at 425-648 °C range with 21.60% weight loss (Calc 21.4%), refers to complete oxidative decomposition of the complex which ended up with the

2043

Eur. Chem. Bull. 2023,12(12), 2026-2058

formation of 2(ZnO)[33].

Complex **(10) [H$_4$L (Pb) $_2$(SO$_4$)$_2$ (H$_2$O)$_2$]. 2H$_2$O** exhibited multiple decomposition steps, the first step involving breaking of H-bonding accompanied with endothermic peak at 45 C^o. In the second step, two molecule of hydrated water were lost endothermically with a peak at 90 C^o accompanied by 3.08% (Calc 3.18%) weight loss. then two molecule of coordinated water were lost endothermically with a peak at 135 C^0 accompanied by 4.5% (Calc %4.55) weight loss.17.5 % (Calc 17.45%) weight loss accompanied by an endothermic peak observed at 217 C^o was assigned to loss of two coordinated sulphate groups (SO$_4$)[35]. The endothermic peak observed at 315°C refers to the melting point of the complex. The final step observed a exothermic peaks at 392-610 ^{0}C range with 49.33% weight loss (Calc 49.28%), refers to complete oxidative decomposition of the complex which ended up with the formation of 2(PbO)[44,45].

Complex **(11) [H$_4$L (Mn) $_2$(CO$_3$)$_2$ (H$_2$O)$_2$]. 2H$_2$O** exhibited multiple decomposition steps, the first step involving breaking of H-bonding accompanied with endothermic peak at 50 C^o. In the second step, two molecule of hydrated water were lost endothermically with a peak at 75 C^o accompanied by 4.7% (Calc 4.47%) weight loss. then two molecule of coordinated water were lost endothermically with a peak at 120 C^0 accompanied by 5% (Calc %4.65) weight loss.17.5 % (Calc 17.45%) weight loss accompanied by an endothermic peak observed at 217 C^o was assigned to loss of two coordinated carbonate groups (CO$_3$). The endothermic peak observed at 350C^o refers to the melting point of the complex. The final step observed a exothermic peaks at 302-600 C^0 range with 25.18% weight loss (Calc 25.65%), refers to complete oxidative decomposition of the complex which ended up with the formation of 2(MnO).

2044

Eur. Chem. Bull. 2023,12(12), 2026-2058

Table 5:- complexes (II)Thermal analyses for metal

Compound No. Molecular formula	Temp. (ºC)	DTA (peak)		TGA (Wt.loss %)		Assignments
		Endo	Exo	Calc	Found	
Complex (2)	30	Endo	-	-	-	Broken of H-bondings
	65	Endo	-	6.2	5.9	Loss of I(3H$_2$O) hydrated water molecule
	285	Endo		28.9	28.7	Loss of coordinated 4(OAc) group
	310	Endo	-	-	-	Melting point
	425,485,598,670	-	Exo	27.37	27.12	Decomposition process with the formation of 2(CuO)
Complex (6)	35	Endo	-	-	-	Broken of H-bondings
	185	Endo	-	4.35	4.20	Loss of (2H$_2$O) hydrated water molecule
	135	Endo	-	4.55	4.5	Loss of (2H$_2$O) coordinated water molecules
	331	Endo	-	25.04	25.43	Loss of coordinated2 (SO$_4$)group
	350	Endo	-	-	-	Melting point
	520,620	-	Exo	25.43	25.2	Decomposition process with the formation of 2(FeO)
Complex (8)	42	Endo	-	-	-	Broken of H-bondings
	70	Endo	-	4.13	4.11	Loss of (2H$_2$O) hydrated water molecules
	235,240	Endo	-	28.29	28.1	Loss of coordinated 4(OAc) group
	350	Endo	-	-	-	Melting point
	425,490,546,648	-	Exo	21.40	21.60	Decomposition process with the formation of 2(ZnO)
Complex (10)	45	Endo	-	-	-	Broken of H-bondings
	90	Endo	-	3.18	3.08	Loss of 2 (H$_2$o) hydrated water molecule
	135	Endo	-	4.5	4.55	Loss of 2(H$_2$o) coordinated water molecule
	217	Endo	-	17.45	17.52	Loss of coordinated 2(SO$_4$) group
	315	Endo	-	-	-	Melting point
	392,481,560,610	-	Exo	49.28	49.33	Decomposition process with the formation of (2PbO)
Complex (11)	50	Endo	-	-	-	Broken of H-bondings
	75	Endo	-	4.47	4.7	Loss of 2(H$_2$O) hydrated water molecule
	120	Endo	-	4.65	5.0	Loss of coordinated 2 (H$_2$O) group
	217	Endo	-	17.5	17.45	LOSS OF 2(CO$_3$)
	350	Endo	-	-	-	Melting point
	392,481,560,600	-	Exo	24.65	25.18	Decomposition process with the formation of (2MnO)

Biological activity

Mammalian cell lines: MCF-7 (breast cancer)were obtained from VACSERA Tissue Culture Unit.

The cytotoxic action of the ligand [H$_4$L] (1) and several of its metal complexes (2-10),) was tested against human breast MCF-7 cancer cells at concentrations ranging from 0.1 to 500 g/L, as shown in figure (2). The IC$_{50}$ values for each compound were determined, and the results are shown in Figure (3) and Table (7). As shown, most complexes had much higher cytotoxic activity as compared to the cisplatin standard. The complexes' cytotoxicity activity can be traced to the central metal atom, as indicated by Tweedy's chelation theory. The highest cytotoxity is the Cu(II) complex

2045

Eur. Chem. Bull. 2023,12(12), 2026-2058

(2) with (IC_{50} = 7.5 M) demonstrated potent cytotoxicity against MCF-7 cancer cells, then Cu (II) complex (4) with (IC_{50} = 8.5 M) against MCF-7 cancer cells, then complexes (7,3) with IC_{50} = 9 M) demonstrated potent cytotoxicity against MCF-7 cancer cells. Complexes (6,8,10) shown moderate cytotoxicity with IC_{50} values of 10-10.5 M, and complexes (9,5) demonstrated the lowest cytotoxicity with IC_{50} values of 21,37 M, respectively. This demonstrated that coordination increased anticancer activity. The positive charge of the metal increased the acidity of the coordinated ligand that bears protons, resulting in stronger hydrogen bonding, which promoted biological activity[13,31]. Changing the anion, coordination sites, and type of the metal ion appears to have a significant effect on biological behaviour through affecting the binding ability of DNA [46]. According to Gaetke and Chow, metal has been proposed to enhance oxidative tissue injury via a free radical mediated route akin to the Fenton reaction [47]. The ESR-trapping approach was used to establish evidence for metal-mediated hydroxyl radical production in vivo[48]. A Fenton-type reaction produces reactive oxygen species as follows:

$LM(II) + H_2O_2$ LM(I) + $^{\cdot}OOH$ + H+ LM(I) + $^{\cdot}OOH$ + H^+

H_2O_2 + LM(I) LM(II) + $^{\cdot}OH$ + OH^-

Where L is an organic ligand

Furthermore, metal may operate as a double-edged sword by both promoting DNA damage and impeding its repair. The OH radicals react with DNA sugars and bases, resulting in the release of free bases and the formation of strand breaks. Hydrogen atom abstraction from the C4 on the deoxyribose unit to give sugar radicals with subsequent -elimination is the most significant and well characterised of the OH reactions. This mechanism causes strand breakage as well as the release of free bases. Solvated electrons damage the DNA bases in a similar way to the reactions detailed below for the direct effects of radiation on DNA [49].
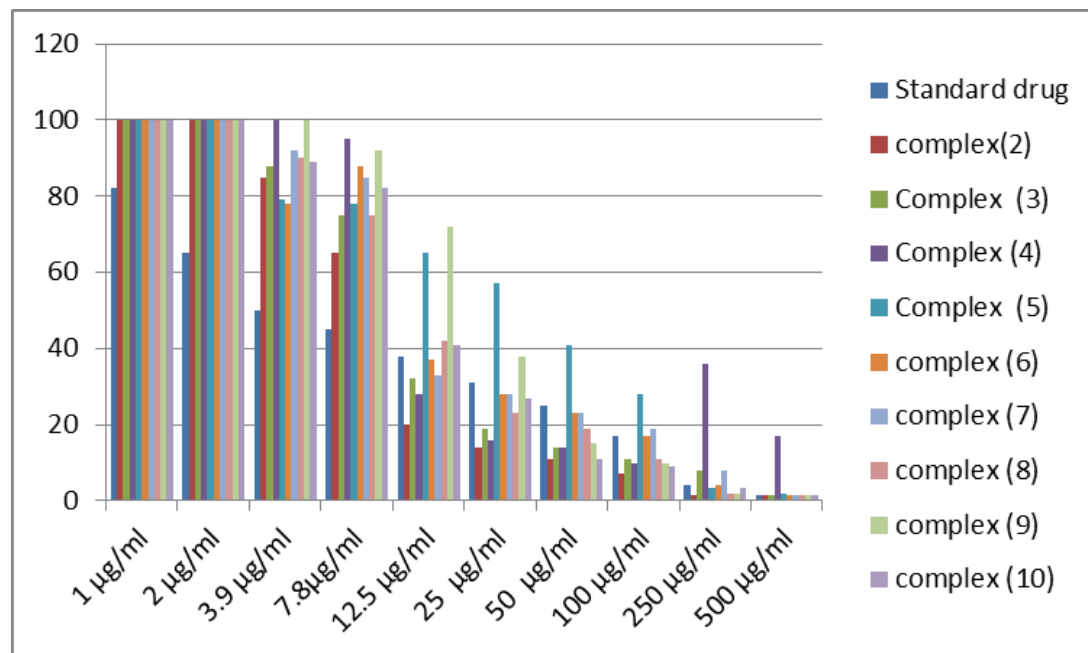
Figure. 2: Mean inhibition zone of metal complexes **(2),(3),(4),(5),(6),(7),(8),(9)** and **(10)** against breast *cancer MCF-7*
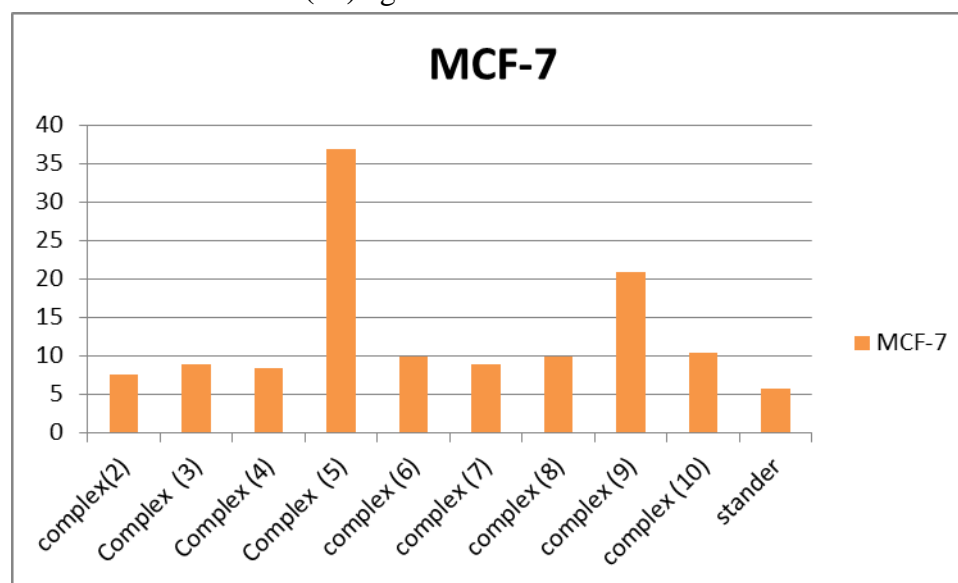
Figure (3): IC_{50} for the metal complexes

2047

Eur. Chem. Bull. 2023,12(12), 2026-2058

Table7:Cytotoxic activity (IC$_{50}$) of some metal complexes against human breast cancere MCF-7.

Compound No.	Compound	(IC$_{50}$)MCF-7 ug)
(2)	[(H$_4$L)(Cu$_2$(OAc)$_4$)].3H$_2$O	7.5
(3)	[(H$_4$L) .Cu$_2$(SO$_4$)$_2$]. 2H$_2$O	9
(4)	[(H4L)(Cu$_2$Cl$_4$)].2H$_2$O	8.5
(5)	[(H$_4$L).(Mn$_2$(OAc)$_4$)].2H$_2$O	37
(6)	[(H$_4$L).(Fe $_2$(SO$_4$)$_2$].2H$_2$O	10
(7)	[(H$_4$L).(Ni $_2$(OAc)$_4$)].2H$_2$O	9
(8)	[(H$_4$L)(.Zn$_2$(OAc)$_4$)] .2H$_2$O	10
(9)	[(H$_4$L).(Zn$_2$ (SO$_4$)$_2$)].2H$_2$O	21
(10)	[(H$_4$L).(Pb$_2$(SO$_4$)$_2$].2H$_2$O	10.5
Standard	Cisplatin	5.71

In vitro studies:

Evaluation of the cytotoxic effect of different complexes on MCF-7 cell line by SRB assay:

Cytotoxicity results indicated that the tested complexes NPs have IC$_{50}$ = 1.63, 7.49, 20.3 and 1.42 μg/ml respectively demonstrated potent cytotoxicity against MCF-7 cancer cells whereas the IC$_{50}$ of the standard drug (cisplatin) was 5.71 μg/ml.

1-Cis platin

2048

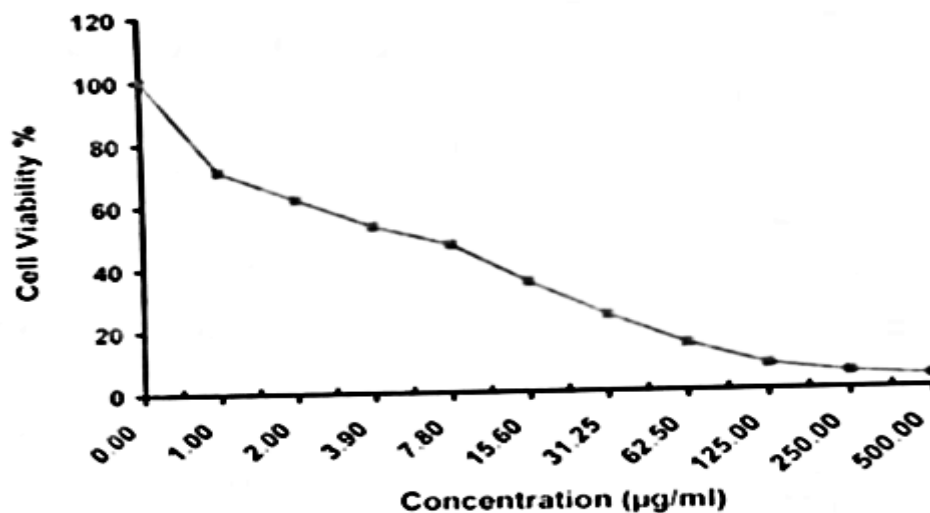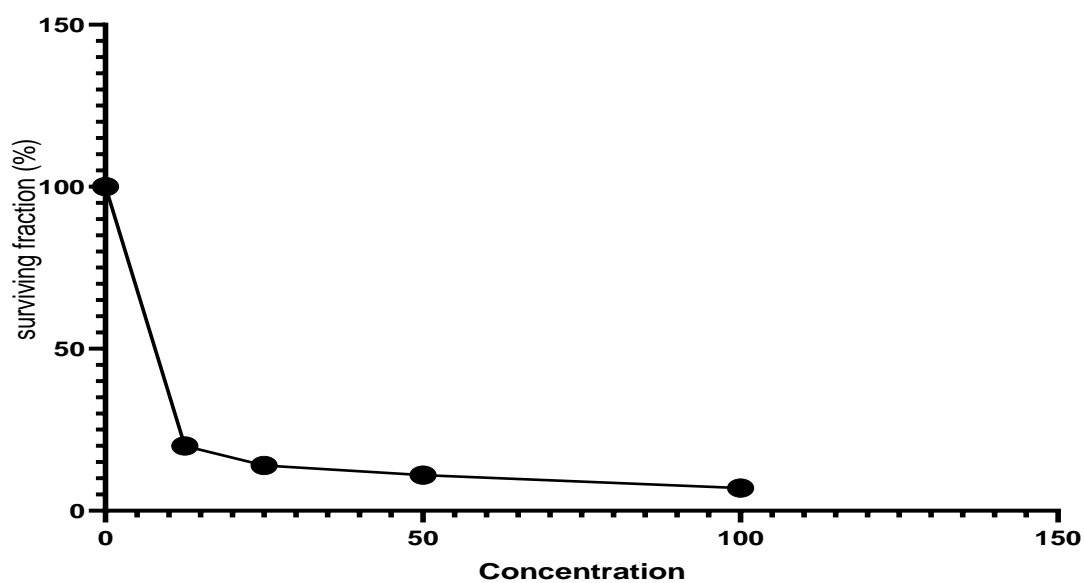*Eur. Chem. Bull. 2023,12(12), 2026-2058*

Figure (4): Mean IC$_{50}$ values of standard drug (Cisplatin) detected by Sulfo-Rhodamine-B-stain (SRB) assay on MCF-7 cell line.
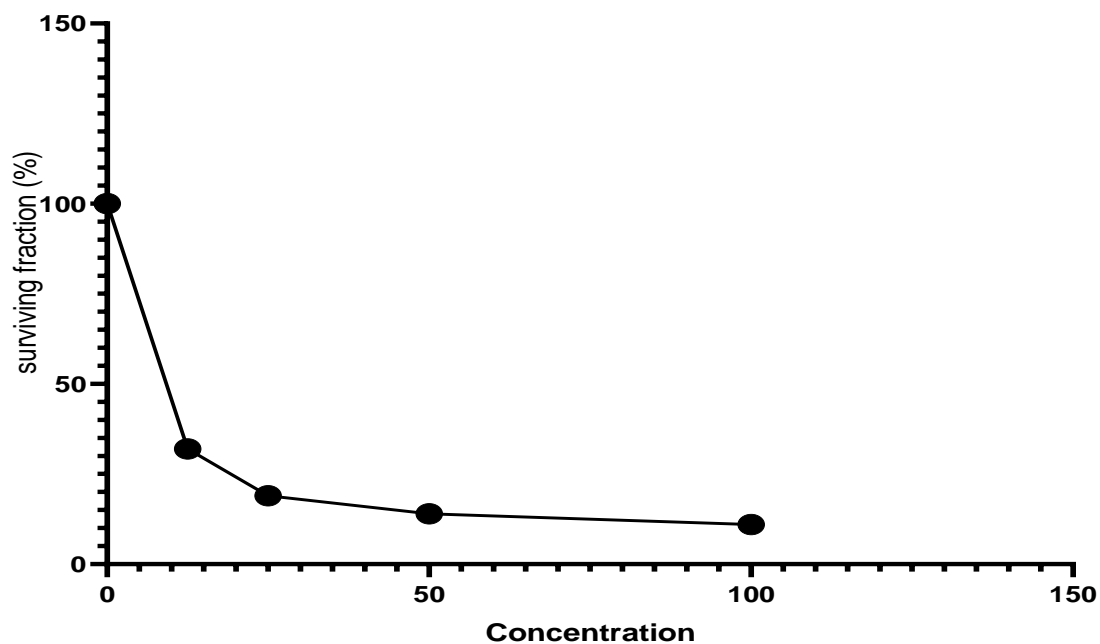
2-Copper acetate

Concentration	Surviving fraction (%)
12.5	20
25	14
50	11
100	7

3- CuSo4

2049

Eur. Chem. Bull. 2023,12(12), 2026-2058

MCF-7

IC50= 9 **ug**

Concentration	Surviving fraction (%)
12.5	32
25	19
50	14
100	11

4-CuCl2

MCF-7

IC50= 8.5 **ug**
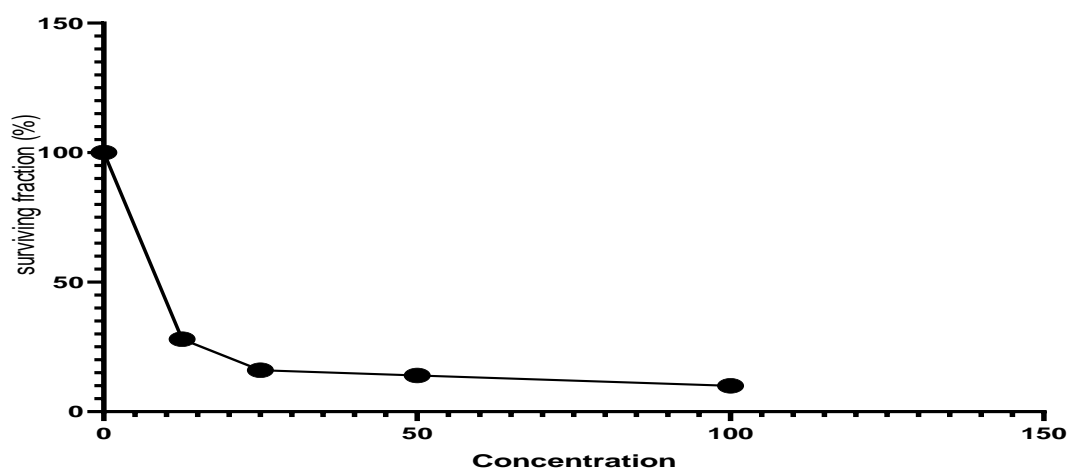
Concentration	Surviving fraction (%)
12.5	28
25	16
50	14
100	10

2050

Eur. Chem. Bull. 2023,12(12), 2026-2058

5- Mn acetate

MCF-7   IC50= 37 **ug**
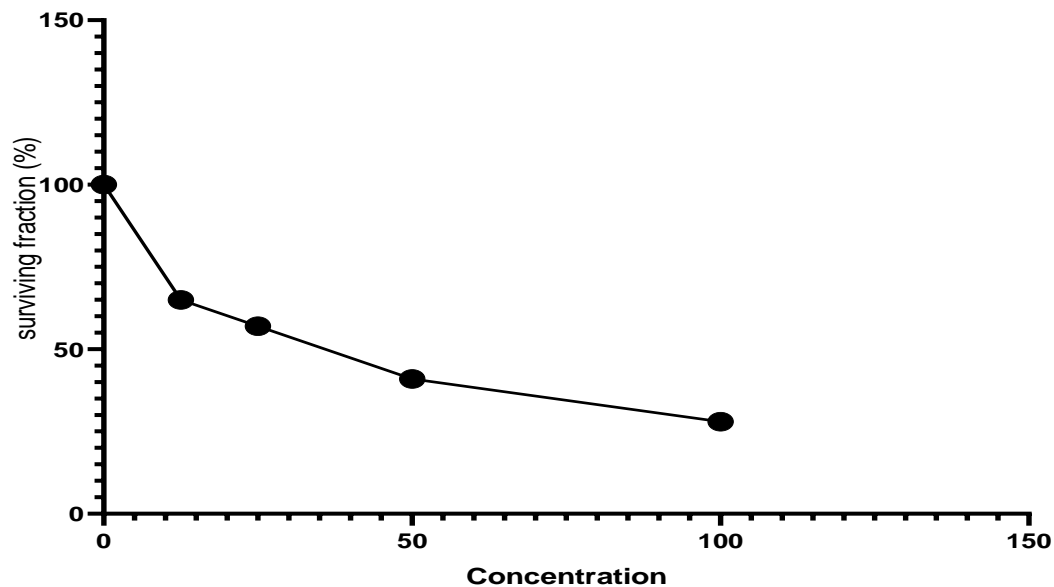
Concentration	Surviving fraction (%)
12.5	65
25	57
50	41
100	28

6- FeSo4

MCF-7   IC50= 10 **ug**
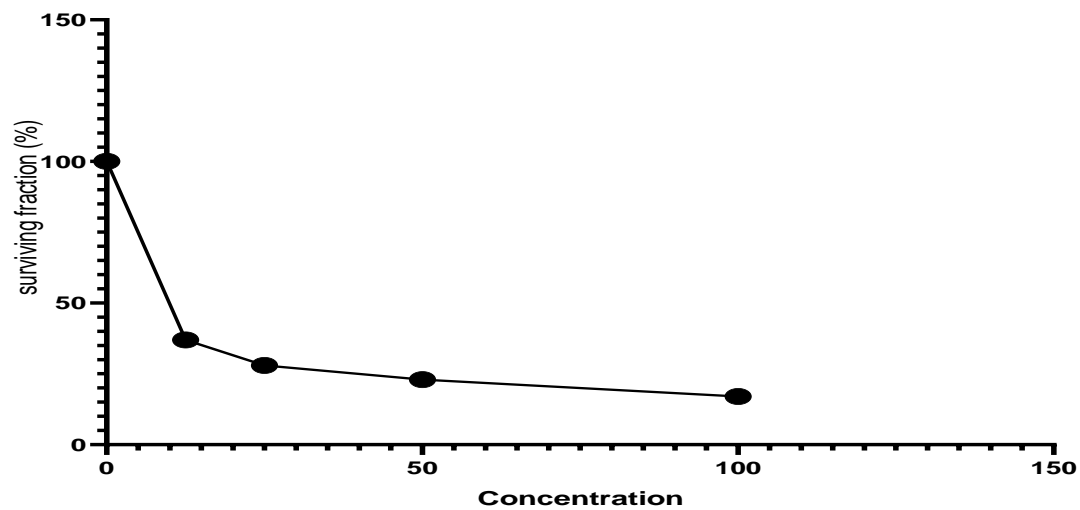
Concentration	Surviving fraction (%)
12.5	37
25	28
50	23
100	17

7- Ni acetate

MCF-7

IC50= 9 **ug**
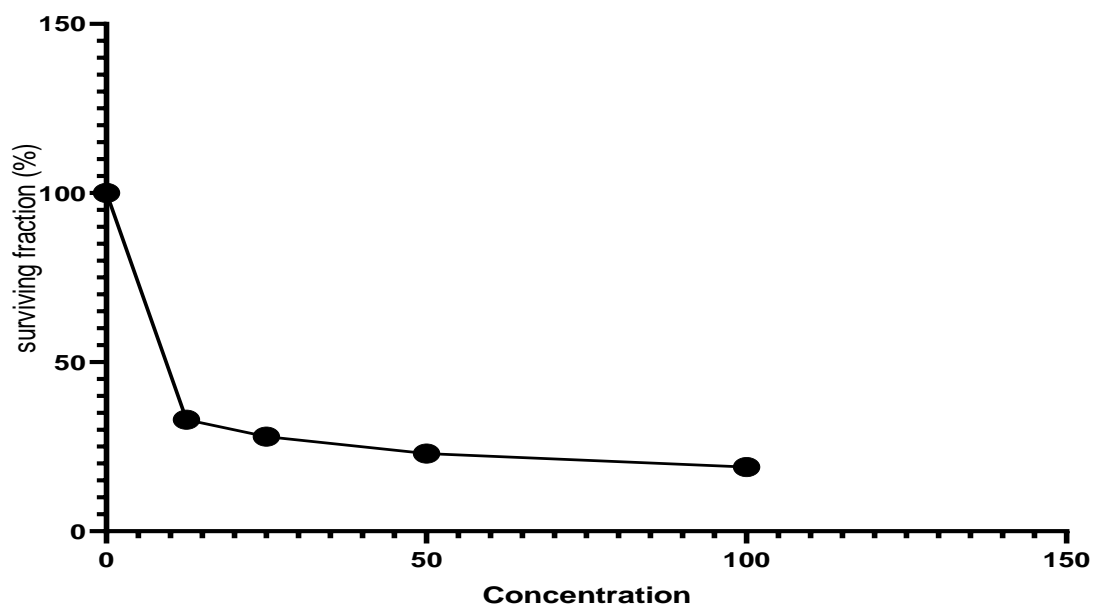
Concentration	Surviving fraction (%)
12.5	33
25	28
50	23
100	19

8-Zn Acetate

MCF-7

IC50=10 **ug**
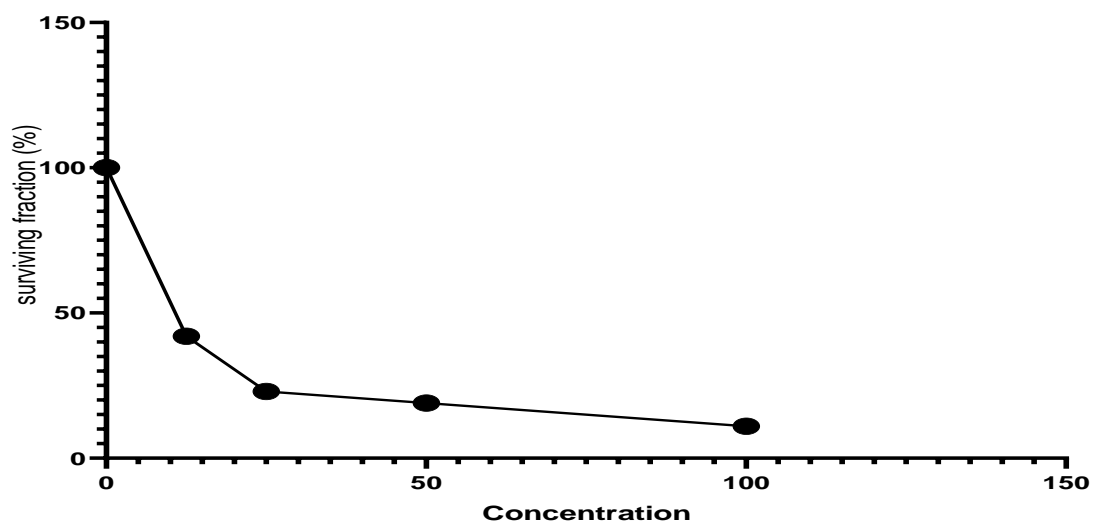
Concentration	Surviving fraction (%)
12.5	42
25	23
50	19
100	11

9-ZnSo4

2052

Eur. Chem. Bull. 2023,12(12), 2026-2058

MCF-7

IC50=21 **ug**
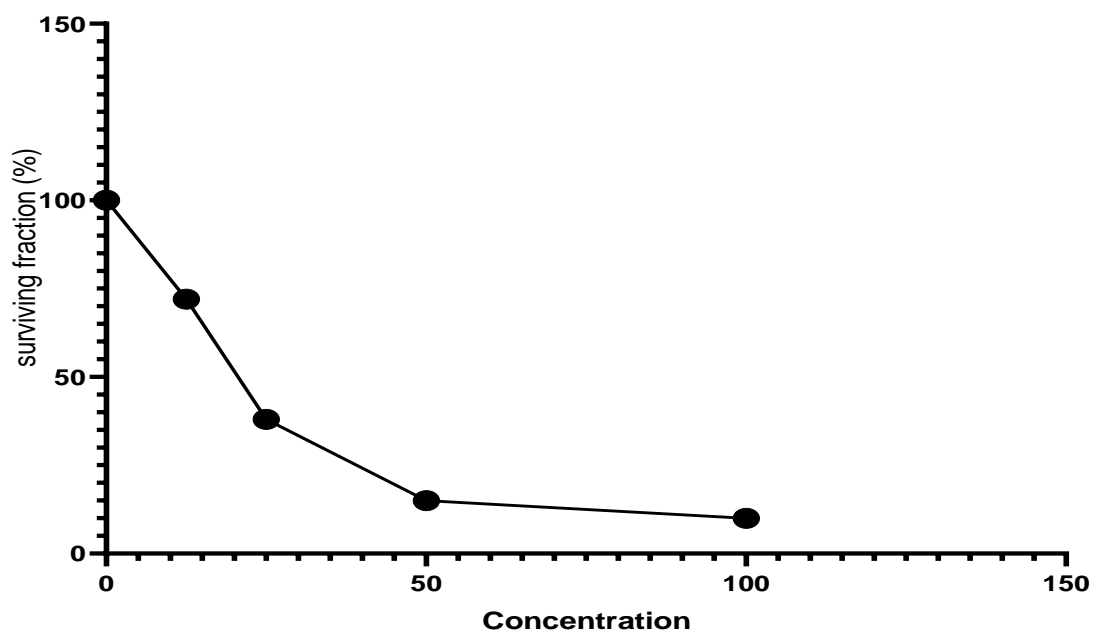
Concentration	Surviving fraction (%)
12.5	72
25	38
50	15
100	10

10-Lead Sulphate

MCF-7

IC50= 10.5 **ug**

Concentration	Surviving fraction (%)
12.5	41

2053

Eur. Chem. Bull. 2023,12(12), 2026-2058
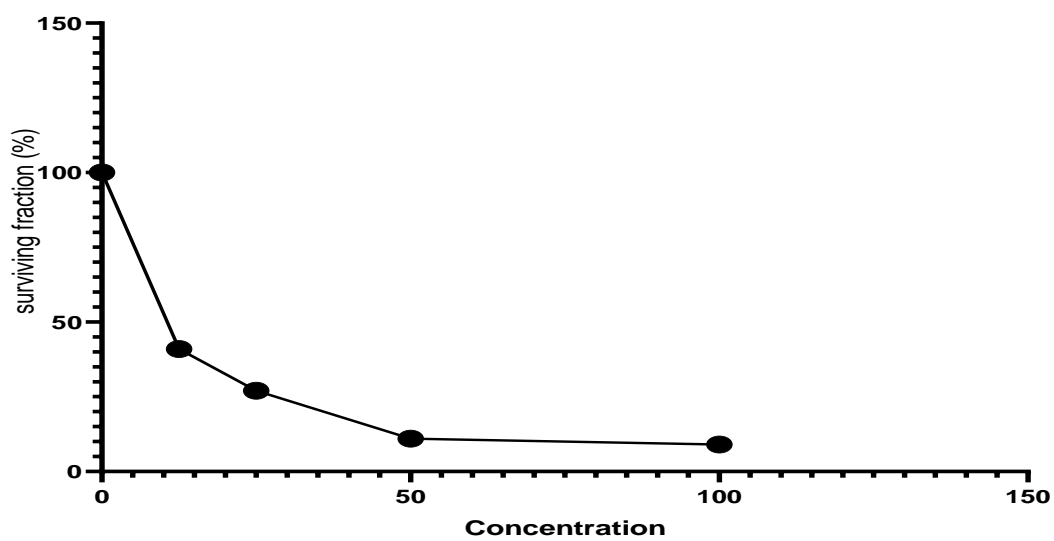
25	27
50	11
100	9

Conclusion

Mono organometallic complexes of Cu(II), Mn(II), Pb(II), Zn(II), Fe(II), and Ni(II) ions with amide ligand((1Z,2Z)N1,N'1,N2,N'2 tetrakis(2hydroxyphenyl)oxalimidamide have significant anticancer potential. These compounds were synthesised and characterised using (^{1}H-NMR, mass, IR, UV-VIS, ESR) spectra, magnetic moments and conductance measurements, elemental and thermal studies. The complexes' antitumor cytotoxicity has been evaluated. Complexes outperform the usual drug. These organometallic complexes are potential anticancer agents.

References

[1].Jahangirian, H., Kalantari, K., Izadiyan, Z., Rafiee-Moghaddam, R., Shameli, K., & Webster, T. J. (2019). A review of small molecules and drug delivery applications using gold and iron nanoparticles. International journal of nanomedicine, 14, 1633..

[2]. Bukowski, K., Kciuk, M., & Kontek, R. (2020). Mechanisms of multidrug resistance in cancer chemotherapy. International journal of molecular sciences, 21(9), 3233.

[3].Abadi, A. J., Mirzaei, S., Mahabady, M. K., Hashemi, F., Zabolian, A., Hashemi, F., ... & Sethi, G. (2022). Curcumin and its derivatives in cancer therapy: Potentiating antitumor activity of cisplatin and reducing side effects. Phytotherapy Research, 36(1), 189-213.

[4].Nam, G. H., Choi, Y., Kim, G. B., Kim, S., Kim, S. A., & Kim, I. S. (2020). Emerging prospects of exosomes for cancer treatment: from conventional therapy to immunotherapy. Advanced Materials, 32(51), 2002440.

[5]. Neidle, S. (2021). Beyond the double helix: DNA structural diversity and the PDB. Journal of Biological Chemistry, 296.

[6].El Tabl, A., Wahed, A. E., Mohamed, E., & Abu-Setta, M. (2021). Modulation of cancer therapy using nano-organometallic compounds: preparation, spectroscopic characterization and cytotoxic evaluation. Egyptian Journal of Chemistry, 64(7), 3873-3887.

[7]. Varghese, N., Jose, J. R., Krishna, P. M., Philip, D., Joy, F., Vinod, T. P., ... & Nair, Y. (2023). In vitro Analytical Techniques as Screening Tools to investigate the Metal chelate- DNA interactions. ChemistrySelect, 8(5), e202203615.

[8]. Xian, S., Lin, Y., Wang, H., & Li, J. (2021). Calcium- Based Metal–Organic Frameworks and Their Potential Applications. Small, 17(22), 2005165.

[9]. Parveen, S., Arjmand, F., & Tabassum, S. (2019). Development and future prospects of selective organometallic compounds as anticancer drug candidates exhibiting novel modes of action. European Journal of Medicinal Chemistry, 175, 269-286.

[10]. Omar, M. A., Ahmed, H. M., Batakoushy, H. A., & Hamid, M. A. A. (2020). New spectrofluorimetric analysis of empagliflozin in its tablets and human plasma using two level full factorial design. Spectrochimica Acta Part A: Molecular and Biomolecular Spectroscopy, 235, 118307.

[11]. Dhanaraj, C. J., & Jebapriya, M. (2020). Metal schiff base complexes of tridentate antipyrine based ligand: Synthesis, spectral characterisation, image analysis and biological studies. Journal of Molecular Structure, 1220, 128596.

[12]. Dhanaraj, C. J., & Jebapriya, M. (2020). Metal schiff base complexes of tridentate antipyrine based ligand: Synthesis, spectral characterisation, image analysis and biological studies. Journal of Molecular Structure, 1220, 128596.

[13]. Alhakimi, A. N. (2020). Synthesis, Characterization and Microbicides Activities of N-(hydroxy-4-((4-nitrophenyl) diazenyl) benzylidene)-2-(phenylamino) Acetohydrazide Metal Complexes. Egyptian Journal of Chemistry, 63(4), 1509-1525.

[14]. El Tabl, A., Wahed, A. E., Mohamed, E., & Abu-Setta, M. (2021). Modulation of cancer therapy using nano-organometallic compounds: preparation, spectroscopic characterization and cytotoxic evaluation. Egyptian Journal of Chemistry, 64(7), 3873-3887.

[15]. El-Tabl, A. S., Shaban, M. T., & Abd El-Wahed, N. M. (2019). Novel metal complexes as antimicrobial agents, synthesis and spectroscopic characterization. Journal of Chemistry and Chemical Sciences, 9(3), 74-108.

[16]. Khalil, E. A., & Mohamed, G. G. (2022). Preparation, spectroscopic characterization and antitumor-antimicrobial studies of some Schiff base transition and inner transition mixed ligand complexes. Journal of Molecular Structure, 1249, 131612.

[17]. Shen, K., Diskin-Posner, Y., Shimon, L. J., Leitus, G., Carmieli, R., & Neumann, R. (2019). Aerobic oxygenation catalyzed by first row transition metal complexes coordinated by tetradentate mono-carbon bridged bis-phenanthroline ligands: intra-versus intermolecular carbon–hydrogen bond activation. Dalton Transactions, 48(19), 6396-6407..

[18]. Schmidbaur, H. (2019). Proof of Concept for Hydrogen Bonding to Gold, Au··· H−X. Angewandte Chemie International Edition, 58(18), 5806-5809.09.

[19]. Fischer, K. C., Sherman, S. L., & Garand, E. (2020). Competition between solvation and intramolecular hydrogen-bonding in microsolvated protonated glycine and β-alanine. The Journal of Physical Chemistry A, 124(8), 1593-1602.

2055

Eur. Chem. Bull. 2023,12(12), 2026-2058

[20].Refat, M. S., Saad, H. A., Gobouri, A. A., Alsawat, M., Adam, A. M. A., Shakya, S., ... & El-Megharbel, S. M. (2022). Synthesis and spectroscopic characterizations of nanostructured charge transfer complexes associated between moxifloxacin drug donor and metal chloride acceptors as a catalytic agent in a recycling of wastewater. Journal of Molecular Liquids, 349, 118121.

[21].Deghadi, R. G., Mohamed, G. G., & Mahmoud, N. F. (2022). Bioactive La (III), Er (III), Yb (III), Ru (III), and Ta (V) complexes of new organometallic Schiff base: Preparation, structural characterization, antibacterial, anticancer activities, and MOE studies. Applied Organometallic Chemistry, 36(6), e6675.

[22]. Cain, Amy N., et al. "Acetate as a model for aspartate-based CXCR4 chemokine receptor binding of cobalt and nickel complexes of cross-bridged tetraazamacrocycles." Dalton Transactions 48.8 (2019): 2785-2801.

[23]. Abdelrhman, E. M., El- Shetary, B. A., Shebl, M., & Adly, O. M. (2021). Coordinating behavior of hydrazone ligand bearing chromone moiety towards Cu (II) ions: Synthesis, spectral, density functional theory (DFT) calculations, antitumor, and docking studies. Applied Organometallic Chemistry, 35(5), e6183.

[24]. Suzuki, A., Moriya, T. J., & Takiwaki, T. (2019). Supernova ejecta interacting with a circumstellar disk. I. Two-dimensional radiation-hydrodynamic simulations. The Astrophysical Journal, 887(2), 249.

[25]. Abd El-Razek, S. E., El-Gamasy, S. M., Hassan, M., Abdel-Aziz, M. S., & Nasr, S. M. (2020). Transition metal complexes of a multidentate Schiff base ligand containing guanidine moiety: Synthesis, characterization, anti-cancer effect, and anti-microbial activity. Journal of Molecular Structure, 1203, 127381.

[26].Conradie, J. (2019). Jahn-Teller effect in high spin d4 and d9 octahedral metal-complexes. Inorganica Chimica Acta, 486, 193-199.

[27].Milam-Guerrero, J., Zheng, M., Spence, N. R., Calder, S., Lapidus, S., & Melot, B. C. (2021). Canting of the Magnetic Moments on the Octahedral Site of an Iron Oxide Garnet in Response to Diamagnetic Cation Substitution. Inorganic Chemistry, 60(9), 6249-6254.

[28].Khalil, E. A., & Mohamed, G. G. (2022). Preparation, spectroscopic characterization and antitumor-antimicrobial studies of some Schiff base transition and inner transition mixed ligand complexes. Journal of Molecular Structure, 1249, 131612.

[29]. El Tabl, Abdou, et al. "Modulation of cancer therapy using nano-organometallic compounds: preparation, spectroscopic characterization and cytotoxic evaluation." Egyptian Journal of Chemistry 64.7 (2021): 3873-3887..

[30].El-Tabl, A. S., Abd-El Wahed, M. M., Shebl, M. A., & Faheem, S. M. (2019). Synthesis, Spectroscopic Characterization and Chemocytotoxic Activity against Hepatocellular

Carcinoma of Novel Metal Complexes. Journal of Chemistry and Chemical Sciences, 9(12), 342-365.

[31]. El Tabl, A., Abd Wlwahed, M., Abd-Elwareth, M., & Faheem, S. (2021). Nano metal complexes in cancer therapy, preparation, spectroscopic, characterization and anti-breast cancer activity of new metal complexes of alanine Schiff-base. Egyptian Journal of Chemistry, 64(6), 3131-3152.

[32]. Asraf, M. A., Rahman, M. M., Kabiraz, D. C., Ansary, R. H., Hossen, M. F., Haque, M. F., & Zakaria, C. M. (2019). Structural elucidation, 3D molecular modeling and antibacterial activity of Ni (II), Co (II), Cu (II) and Mn (II) complexes containing salophen ligand. Asian Journal of Applied Chemistry Research, 3(3), 1-15.

[33].NB, G. R., & Murali Krishna, P. Chloro Bridged Binuclear Copper (Ii) Complexes of 4n-Substituted Hydrazine Carbothioamides: Synthesis, Spectral Characterisation and Their Biological Applications.

[34]. Jyothi, N., Ganji, N., & Daravath, S. (2020). Mononuclear cobalt (II), nickel (II) and copper (II) complexes: Synthesis, spectral characterization and interaction study with nucleotide by in vitro biochemical analysis. Journal of Molecular Structure, 1207, 127799.

[35].Jyothi, N., Ganji, N., & Daravath, S. (2020). Mononuclear cobalt (II), nickel (II) and copper (II) complexes: Synthesis, spectral characterization and interaction study with nucleotide by in vitro biochemical analysis. Journal of Molecular Structure, 1207, 127799.

[36].Serhan, C. N., Libreros, S., & Nshimiyimana, R. (2022, January). E-series resolvin metabolome, biosynthesis and critical role of stereochemistry of specialized pro-resolving mediators (SPMs) in inflammation-resolution: Preparing SPMs for long COVID-19, human clinical trials, and targeted precision nutrition. In Seminars in Immunology (Vol. 59, p. 101597). Academic Press.

[37].Emam, S. M., Abouel- Enein, S. A., & Abdel- Satar, E. M. (2019). Structural characterization, thermal investigation and biological activity of metal complexes containing Schiff Base ligand (Z)- 3- (1- ((4, 6- dimethyl- 1H- pyrazolo [3, 4- b] pyridin- 3- yl) imino) ethyl)- 4- hydroxy- 6- methyl- 2H- pyran- 2- one. Applied Organometallic Chemistry, 33(5), e4847.

[38]. Hosny, N. M., Hassan, N. Y., Mahmoud, H. M., & Abdel- Rhman, M. H. (2019). Synthesis, characterization and cytotoxicity of new 2- isonicotinoyl- N- phenylhydrazine- 1- carbothioamide and its metal complexes. Applied Organometallic Chemistry, 33(8), e4998..

[39].Konakanchi, R., Pamidimalla, G. S., Prashanth, J., Naveen, T., & Kotha, L. R. (2021). Structural elucidation, theoretical investigation, biological screening and molecular

docking studies of metal (II) complexes of NN donor ligand derived from 4-(2-aminopyridin-3-methylene) aminobenzoic acid. Biometals, 34, 529-556..

[40]. Chang, H. C., Mondal, B., Fang, H., Neese, F., Bill, E., & Ye, S. (2019). Electron paramagnetic resonance signature of tetragonal low spin iron (V)-nitrido and-oxo complexes derived from the electronic structure analysis of heme and non-heme archetypes. Journal of the American Chemical Society, 141(6), 2421-2434.

[41].Shakdofa, M. M., Morsy, N. A., Rasras, A. J., Al- Hakimi, A. N., & Shakdofa, A. M. (2021). Synthesis, characterization, and density functional theory studies of hydrazone–oxime ligand derived from 2, 4, 6- trichlorophenyl hydrazine and its metal complexes searching for new antimicrobial drugs. Applied Organometallic Chemistry, 35(2), e6111..

[42]. Abd El-Razek, Samar Ebrahim, et al. "Transition metal complexes of a multidentate Schiff base ligand containing guanidine moiety: Synthesis, characterization, anti-cancer effect, and anti-microbial activity." Journal of Molecular Structure 1203 (2020): 127381.

[43].Brunner, M. (2021). Ionic Liquids for Biomass Dissolution and Analysis of Their Solvent Properties.

[44].Ghosh, S., Kundu, S., & Naskar, M. K. (2021). Mesoporous CuO nanostructures for low-temperature CO oxidation. Bulletin of Materials Science, 44(3), 189.

[45].Al-Bayaty, S. A., Jubier, N. J., & Al-Uqaily, R. A. (2020). Study of thermal decomposition behavior and kinetics of epoxy/polystyrene composites by using TGA and DSC. Journal of Xian University of Architecture & Technology, 12(3), 1331-1341.

[46]. Orysyk, S. I., Baranets, S., Borovyk, P. V., Palchykovska, L. G., Zborovskii, Y. L., Orysyk, V. V., ... & Vovk, M. V. (2021). Mononuclear π-complexes of Pd (II) and Pt (II) with 1-allyl-3-(2-hydroxyethyl) thiourea: Synthesis, structure, molecular docking, DNA binding ability and genotoxic activity. Polyhedron, 210, 115477.

[47]. Gaun, S., Ali, S. A., Singh, P., Patwa, J., Flora, S. J. S., & Datusalia, A. K. (2023). Melatonin ameliorates chronic copper-induced lung injury. Environmental Science and Pollution Research, 30(10), 24949-24962.

[48]. El-Tabl, A. S., Abd-El Wahed, M. M., El-Azm, M. I. A., & Faheem, S. M. (2020). Newly Designed Metal-based Complexes and their Cytotoxic Effect on Hepatocellular Carcinoma, Synthesis and Spectroscopic Studies. Journal of Chemistry and Chemical Sciences, 10(1), 10-31.

[49]. Zdrowowicz, M., Chomicz-Mańka, L., Butowska, K., Spisz, P., Falkiewicz, K., Czaja, A., & Rak, J. (2022). DNA Damage Radiosensitizers Geared Towards Hydrated Electrons. Practical Aspects of Computational Chemistry V, 125-169.

2058

Eur. Chem. Bull. 2023,12(12), 2026-2058